Journal of Materials Chemistry C

Accepted Manuscript

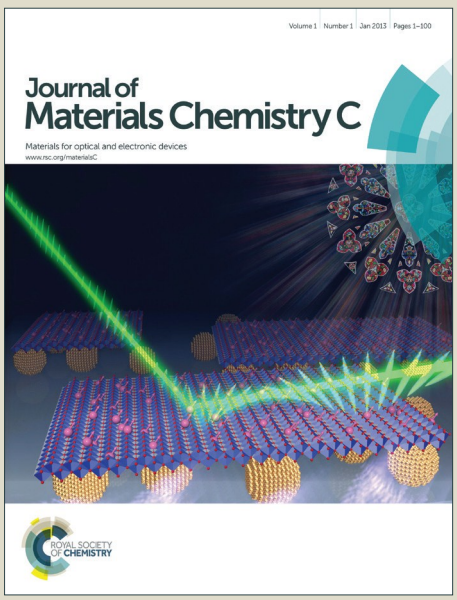

ROYAL SOCIETY OF CHEMISTRY

www.rsc.org/materialsC

Fully transparent thin–film varactors: fabrication and performance

Shihui Yu[a], Lingxia Li[a*], Weifeng Zhang[b], Zheng Sun[a] , Haoran Zheng[a]

[a]*School of Electronic and Information Engineering, Tianjin University, Tianjin 300072, P. R. China*

[b]*Key Laboratory of Photovoltaic Materials of Henan Province and School of Physics and Electronics, Henan University, Kaifeng 475004, P. R. China*

Abstract

We report the fabrication of fully transparent thin–film varactors using a dielectric material, barium strontium titanate ($Ba_{0.6}Sr_{0.4}TiO_3$, BST), as an electric field tunable layer, transparent conductive oxide (Sb doped SnO_2, ATO) as a bottom electrode and ATO/Ag tri–layer film as a top electrode. This kind of varactors using ATO/Ag/BST/ATO capacitors shows a transmittance of about 80% (including the substrate) in the visible region, a medium capacitance of about 463 pF, low loss tangent of about 0.015, and superior tunable dielectric properties at room temperature. Calculations of dielectric tunability and figure of merit (FOM) display a maximum value of ~53% at 560 kV/cm and ~66, respectively. We believe that the transparent thin–film varactors using ATO/Ag/BST/ATO capacitors presented in this paper could be a milestone for future see–through electronic devices.

Keywords: Thin films; Varactors; X–ray diffraction; Transparent; BST

1. Introduction

* Corresponding author. Tel./fax: +86 2227402838.
E-mail address: lingxiali@126.com (L. Li).

Transparent electronic circuits are expected to serve as the basis for new optoelectronic devices [1–3]. The key for realizing transparent circuits is the transparent electronic device design [4–5]. So far, mainly transparent electronic devices such as transistors and diodes have been investigated [6–8]. However, studies on transparent thin–film varactors (TTFVs), which are indispensable for invisible electronics, are still lacking, owing to the limit of transparent p–type semiconductor [9–10]. Here, we propose to solve this problem by using a novel structure—a sandwich structure of transparent electrode /tunable material/ transparent electrode. The barium strontium titanate ($Ba_xSr_{1-x}TiO_3$, BST) would be used as tunable material due to BST thin films deposited on Pt–Si substrate exhibit large tunability (>40%) at room temperature and a wide optical bandgap (>3.0 eV) [11–12].

Transparent electrodes are widely used in optical–electronic devices such as solar cells, displays, organic light–emitting diodes (OLED), and touch screens. In these devices, indium tin oxide (ITO) has been commonly used as a transparent electrode [13–15]. The ITO electrode has many merits such as optical transparency, electrical conductivity and environmental stability. With the rapid growth of the display industry, the demand for transparent electrodes has increased dramatically. Accordingly, the exhaustion of the world's indium supply has become an important issue, and the growth of industrial demand has stimulated the rationing of rare–earth metal resources [16]. Therefore, many alternatives to ITO have been developed for use as transparent electrodes. Impurity–doped tin oxide (SnO_2) thin films as TCO films have received much attention because it is nontoxicity, cheap and abundant

elements. Sb and F are found to be the most commonly used dopants for photovoltaic devices in terms of a manufacturing point of view [17–18]. Among these, Sb has been shown to be effective and low cost, which becomes an attractive material [19]. Yet, for some advanced practical applications such resistivity values are rather high. Recently, electrical resistivity has been further improved by embedding a thin metal film. Among metals, Ag is a good candidate for such multilayer films because of its low resistivity. As alternative processes, Sb–doped SnO_2 (ATO)/Ag multilayer films has raised an interest due to its low resistivity and high transmittance in the visible region [20]. With advances in the development of transparent electrodes, preparation of may be feasible by using transparent electrodes. In this paper, we report fabrication and performance of TTFVs fabricated using BST as a tuning material layer. TTFVs of ATO/Ag/BST/ATO were prepared by pulsed laser deposition with a KrF excimer laser and magnetron sputtering, using a 20 at% Sb doped SnO_2 target, a polycrystalline $Ba_{0.6}Sr_{0.4}TiO_3$ target and a metal Ag target. The schematic drawings of the fully transparent thin–film varactors are shown in Fig. 1a.

2. Experimental

In order to prepare the ATO/Ag/BST/ATO varactors, the $Ba_{0.6}Sr_{0.4}TiO_3$ ceramic target was prepared by solid state reaction process with TiO_2, $BaCO_3$ and $SrCO_3$ as starting materials. The mixed powder was pressed at 20 ton and sintered at 1400 ℃ for 5 h in air to fabricated BST ceramic target. The deposition conditions of ATO/quartz substrates have been described in our previous work [21]. The 180 nm thick $Ba_{0.6}Sr_{0.4}TiO_3$ thin films were deposited on ATO/ quartz glass substrates by

pulsed laser deposition from the BST ceramic target in O_2 ambient gas at 700 °C. The total pressure during deposition was maintained at 10 Pa. After the deposition, BST thin films were post–annealed at 750 °C for 10 min in oxygen ambient oven, the total pressure during annealing was maintained at 0.02 MPa with a flow rate of 50 sccm. In order to obtain a fully transparent metal/insulator/metal structure, we used an ATO/Ag top electrode with a 200–μm diameter. The deposition conditions of ATO (40 nm) /Ag (9 nm) top electrodes have been described in our previous work [20]. The schematic configurations of the final device were shown in Figure 1a. The as–deposited BST thin films and annealed BST thin films were used as insulators of varactors, respectively.

The crystal structure of the BST thin films was characterized by X–ray diffraction (Rigaku D/MAX–RB, Akishima, Tokyo, Japan). The thickness of the thin films was measured by Alpha–Step D–100 profilometer (KLA–Tencor, California, USA). The capacitance–voltage (C–V) characteristics were measured at the frequency of 100 kHz with a small ac signal amplitude of 0.2 V by Aglient 4285A precision LCR meter (Santa Clara, California, USA), while the dc bias voltage was swept from negative bias (–10 V) to positive bias (+10 V), the relatively tunability (n_r) in bias field was defined as

$$n_r = \frac{C(0)-C(\upsilon)}{C(0)} \quad (1)$$

where $C(0)$ is the measured capacitance at zero bias field and $C(\upsilon)$ is the capacitance at a certain bias field. The dielectric properties were measured at room temperature was examined by LCR analyzer (TH2828S, Tonghui Electronics, Shenzhen, China).

The leakage current of the films was measured by Aglient 4339B High Resistance Meter (Santa Clara, CA, USA) at room temperature, while the dc bias voltage was swept from 0 V to 10 V (increment 0.25 V). The ferroelectric hysteresis was measured using a Radiant Precision LC 2000 System. Optical transmittance spectra were obtained on an ultraviolet–visible–near infrared (UV–Vis–NIR) spectrophotometer (Cary 5000, Varian).

3. Results and discussion

The X–ray diffraction (XRD) spectra for the BST (150 nm)/ATO samples in order to examine their structural properties using a set of joint committee on powder diffraction standards cards. As shown in Fig. 1b. The two kinds of BST thin films (as–deposited and annealed BST thin films) both show a single phase with perovskite structured [22], without any other noticeable phase. It should be noted that there was a slight shift of the x–ray peaks for the annealed BST thin films to higher angle (corresponding to smaller interplanar spacing) with respect to that of the as–deposited BST thin films. This downshift in the peak position is indicative of the fact that the lattice parameter ($a_{annealed}$ =3.92 Å) of the annealed BST thin films, based on the (110) x–ray peak was slightly smaller than that ($a_{as–deposited}$=3.95 Å) of the as–deposited thin films. Oxygen vacancies affect the nearest neighbor distance by reducing the Coulomb attractive force between cations and anions, resulting in an increased lattice parameter [23]. For the as–deposited BST thin films, the vacuum deposited lead to the formation of a large number of oxygen vacancy related defect states in the thin films, the oxygen vacancy site has a net positive value thus repelling the Ba, Sr, and Ti

atoms causing a distortion in the lattice parameter.[23] The influx of activated oxygen during annealing allows for a greater compensation of the vacancies likely resulting in the reduction of the lattice parameter, and ultimately alleviating thin film strain by filling oxygen vacancies. Therefore, the annealed thin films display structural characteristics closer to that of bulk BST, i.e., lattice parameter closer to bulk with respect to the as–deposited BST thin films, advocating a reduction in thin film stress resultant of defect (oxygen vacancies) annihilation in the film with respect to the as–deposited thin films [24].

Fig. 2a shows the spectral transmission curves of the two sets of BST thin films grown on the ATO/quartz glass substrates. All the transmission spectra show interference fringes arise from intereference between reflections at the air and substrate thin film interfaces, indicate that the thin films have smooth surfaces and interfaces. The sharp fall in transmission and disappearance of the fringes at the shorter wavelength is due to the fundamental absorption of the thin films. Average transmittance (T_{av}) can be defined as follows [25]:

$$T_{av} = \frac{\int V(\lambda)T(\lambda)d\lambda}{\int V(\lambda)d\lambda} \quad (2)$$

where T(λ) is the measured transmittance of thin film system, and V(λ) is the photopic luminous efficiency function defining the standard observer for photometry. The range of λ is from 380 nm to 780 nm. V(λ) approaches zero beyond this region and reaches the maximum of 1 at 555 nm, the medium of this region. The optical transmittance of as–deposited BST thin films is about 84% in the visible range of wavelengths (380–780 nm). We can see that the annealed BST thin films show high

transmittance (about 86%) in the visible region. The increase of the optical transmittance of BST thin film after annealed can be attributed to a weakening of the scattering, and the absorption of light, due to the decrease of oxygen vacancies and the increase of the crystallinity. The optical band gap *(Eg*) estimated from the Tauc relationship [26]:

$$ahv=C(hv–Eg)^{n} \quad (3)$$

where C is a constant, *v* is the transition frequency and the exponent n characterizes the nature of band transition. n = 1/2 and 3/2 corresponds to direct allowed and direct forbidden transitions and n = 2 and 3 corresponds to indirect allowed and indirect forbidden transitions, respectively. Inter–band optical transitions that can be described by wave functions localized over a distance of the order of lattice constant are relatively unchanged by disorder. Therefore, optical band gap and the constant *C* estimated from $\alpha^{1/n}$ vs *Eg* reflects its local atomic structure undetected by XRD. That is, these parameters can be correlated with the short–range order at the nano–scale and, particularly, amorphous phase alone or phases co–existing with crystalline materials in thin films. It is observed that for all the films, the best straight line is obtained for n = 1/2 which is expected for direct allowed transitions. The optical band gap of as−deposited BMN thin film obtained from Fig. 2b is 3.45 eV. After annealed at 700 °C, the optical band gap increase to 3.67 eV. The low band gap in the as–deposited BST thin films may be due to the disorder crystalline structure and the increase in optical band gap what reflects the crystallinity in the BST thin films.

The optical transmittance of a TTFVs composed of quartz glass, a 300 nm thick

bottom ATO layer, a 150 nm thick BST layer, a 9 nm thick Ag layer and a 40 nm thick top ATO layer was measured, as shown in of Fig. 2c. The average optical transparency of the TTFVs with annealed BST thin films including the quartz glass substrate is approximately 80% in the visible wavelength region from 380 to 780 nm. In general, we think that this result can be immediately applied to fully transparent electric–field tunable devices.

The applied bias field dependent capacitance of the two sets of fully transparent thin–film varactors (with as–deposited and annealed BST thin films) was measured. It turns out that a large tunability of ~50% can be achieved in a repeatable manner for the TTFVs with annealed BST thin films. Figure 3 shows the bias field dependent capacitance and loss tangent of the two sets of TTFVs measured at 100 kHz. The capacitance (437 pF) of the TTFVs with as–deposited BST thin films are slightly lower than that of the TTFVs with annealed (463 pF). This may be related to the lattice parameter difference in the two samples as the ionic displacement is reduced lowering the net polarization [27]. The capacitance for both sets of thin films is reasonable (i.e., C <500 pF), for device impedance matching purposes [28–29], thereby allowing efficient power transfer in the device. What is also important in Figure 3 is the tunability data. Comparing with the tunability of TTFVs with as as–deposited BST thin films, which is about 45.7% at the bias field of 560 kV/cm, the tunability of the TTFVs with annealed BST thin films has a large improvement up to ~53% at bias applied bias field 560 kV/cm. These results can be qualitatively interpreted by the phenomenological theory of Devonshire and the simplified

expression proposed by Johnson [30]:

$$C(v) = \frac{C(O)}{[1+\beta_{(T)}E^2]^{1/3}} \quad (4)$$

where $\beta_{(T)}$ is a temperature–dependent constant given by

$$\beta_{(T)} = \left[\frac{C(0)d}{S}\right]^3 \alpha_{(T)} \quad (5)$$

where $\alpha_{(T)}$ is a temperature–dependent constant that provides information on the degree of anharmonic contributions of the polarization to the free energy [31], *d* is the thickness of BST thin films, and *S* is the area of ATO/Ag transparent electrodes. The experimental data of *C*–*E* at 100 kHz and room temperature are fitted using Eq. (1), as represented by the solid lines. As shown in Fig. 3, the *C*–*E* curves can be fitted well over the whole electric field range. Combined with Eqs (1), (4) and (5), the dielectric tunability can be written as

$$n_r = 1 - \frac{1}{[1+\beta_{(T)}E^2]^{1/3}} \quad (6)$$

Eq. (6) demonstrates that the larger the $\beta_{(T)}$ value, the larger the dielectric tunability would be. Therefore, it is predicted that the higher the value of capacitance at zero electric field, the larger the dielectric tunability would be. The slight asymmetric characteristic of the C–V curves of the BST thin films should be noticed. Well–defined ferroelectric hysteresis loops were obtained for the annealed thin films, as shown in Fig. 3c, which indicate that the BST thin films are ferroelectric at room temperature.

In electrically tunable applications, the figure of merit (FOM) is usually used to evaluate the quality of TTFVs. The FOM is defined as [28–29]:

$$\text{FOM} = \frac{Tunability}{tan\delta} \quad (7)$$

where *tan δ* is the loss tangent. The value of FOM in the TTFVs is calculated according to Eq. (7). The value of FOM in the Au/$Ba_{0.5}Sr_{0.5}TiO_3$/Pt and Au//$Ba_{0.5}Sr_{0.5}TiO_3$/Au varactors were also calculated, respectively. The results are summarized in Table I. It is seen that the value 66 of the TTFVs with annealed BST is greater than that 47 of Au/$Ba_{0.6}Sr_{0.4}TiO_3$/Au varactors and 35 of Au/$Ba_{0.5}Sr_{0.5}TiO_3$/Pt varactors.

As shown in Fig. 3a and b, in contrast to TTFVs with as–deposited BST thin films, the TTFVs with annealed BST thin films have significantly lower loss tangent. The factors influencing the dielectric loss are quite complicated. However, at low frequency considered in this study, the overall dielectric loss is dedicated by the polarization loss (it is strongly affected by space dipole determined by interface conditions and defects in BST thin films) and leakage conductance loss. The leakage conductance loss was evaluated by leakage current measurements. And, leakage current is also one of the limiting factors for the suitability of a dielectric material for filter/tunable device applications [33]. It has been argued that the major factors that influence leakage characteristics of TTFVs are oxygen vacancies generated during deposition of the BST thin films and during sputtering of the top electrode, and mechanical damage imposed by sputtering of the top electrode [34]. The relation of the leakage current density versus the applied bias is shown for the two sets of fully transparent thin–film varactors in Figure 3C. The value of leakage current density is 1.2×10^{-3} A/cm^2 for the TTFVs with as–deposited BST thin films at a bias field of 560 kV/cm. The value of leakage current density is 5.9×10^{-4} A/cm^2 for the TTFVs with

annealed BST thin films at the same field, which almost half lower than that of TTFVs with as–deposited thin films. The oxygen vacancies generated at the top BST electrode by the sputtering process as well as the oxygen vacancies in the film from the initial sputtering conditions may act as electron trap sites causing high leakage currents in the capacitor. Since the annealing increases the influx of oxygen through the BST thin films, the vacancies are annihilated and thus the leakage current is decreased.

Capacitance (C) and loss tangent ($tan\ \delta$) are important for the functioning of thin–film varactors. The capacitance and dielectric loss were measured by applying a small ac signal of 0.2 V amplitude as a function of frequency in the range of 1 kHz–30 MHz. Figure 4b gives the frequency dependence on the capacitance and dielectric loss of the TTFVs with annealed BST thin films. It was observed that the capacitance does not show noticeable variation, it only decreases by 6% in the measured frequency range. The capacitance almost independent of frequency suggests that there were few oxygen vacancies at the Ag/BST interface [35]. It also was observed that loss tangent for the capacitance remained essentially constant around 0.015 in the frequency range of 1 kHz ~ 300 kHz. As the frequency increases beyond 300 kHz, the loss tangent increases with frequency. A strong increase of loss tangent is observed at a high frequency of >10 MHz, which is extrinsic in nature due to the resonance of the equivalent circuit. At frequencies on the order of a MHz, the stray inductance of the contact and the leads may induce L−C resonance ($f_r = \frac{1}{\sqrt{LC}}$) [36], where L and C are the inductance and the capacitance of the equivalent circuit, respectively. For the TTFVs having capacitances on the order of 100 pF or so (as in the present case), a stray in–ductance on the order of a few μH can induce resonance in the MHz range.

This seems to be the reason for the strong increase of loss tangent at the high frequency of 10 MHz since such resonance behavior starts around 10 MHz. In the measurement range, the dielectric loss is generally stable and less than 0.035, however, for potential microwave applications, the capacitance and loss tangent at microwave frequencies should be further explored.

4. Conclusions

In summary, we report the fabrication of fully transparent thin–film varactors using a dielectric material, barium strontium titanate ($Ba_{0.6}Sr_{0.4}TiO_3$, BST), as an electric field tunable layer, transparent conductive oxide (Sb doped SnO_2, ATO) as a bottom electrode and ATO/Ag tri–layer film as a top electrode. This kind of varactors using ATO/Ag/BST/ATO capacitors shows a transmittance of about 80% (including the substrate) in the visible region, a medium capacitance of about 463 pF, low loss tangent of about 0.015, and superior tunable dielectric properties at room temperature. Calculations of dielectric tunability and figure of merit (FOM) display a maximum value of ~53% at 560 kV/cm and ~66, respectively. We believe that the transparent thin–film varactors using ATO/Ag/BST/ATO capacitors presented in this paper could be a milestone for future see–through electronic devices.

Acknowledgments

This work was supported financially by Program for New Century Excellent Talentsin University (NCET), 863 Program (2007AA03Z423) and the Program for Innovative Research Team in Science and Technology in University of Henan Province (IRTSTHN) (Grant No. 2012IRTSTHN004).

References

[1] J. F. Wager, *Science*, 2003, **300**, 1245.

[2] K. Nomura, H. Ohta, A. Takagi, T. Kamiya, M. Hirano and H. Hosono, *Nature*, 2004, **432**, 488.

[3] K. Nomura, H. Ohta, K. Ueda, T. Kamiya, M. Hirano and H. Hosono, *Science*, 2003, **300**, 1269.

[4] T. Georgiou, R. Jalil, B. D. Belle, L. Britnell, R. V. Gorbachev, S. V. Morozov, Y. J. Kim, A. Gholinia, S. J. Haigh, O. Makarovsky, L. Eaves, L. A. Ponomarenko, A. K. Geim, K. S. Novoselov and A. Mishchenko, *Nat. Nanotechnol.*, 2013, **8**, 100.

[5] W. J. Yu, S. H. Chae, S. Y. Lee, D. L. Duong and Y. H. Lee, *Adv. Mater.*, 2011, **23**, 1889.

[6] J. Jang, R. Kitsomboonloha, S. L. Swisher, E. S. Park, H. Kang and V. Subramanian, *Adv. Mater.*, 2013, **25**, 1042.

[7] Y. Yuan, G. Giri, A. L. Ayzner, A. P. Zoombelt, S. C. B. Mannsfeld, J. Chen, D. Nordlund, M. F. Toney, J. Huang and Z. Bao, *Nat. Commun.*, 2014, **5**, 3005.

[8] Y. H. Kim, J. Lee, S. Hofmann, M. C. Gather, L. Müller–Meskamp and K. Leo, *Adv. Funct. Mater.*, 2013, **23**, 3763.

[9] G. Hautier, A. Miglio, G. Ceder, G. M. Rignanese and X. Gonze, *Nat. Commun.*, 2013, **4**, 2292.

[10] L. Liu, J. Xu, D. Wang, M. Jiang, S. Wang, B. Li, Z. Zhang, D. Zhao, C. X. Shan, B. Yao and D. Z. Shen, *Phys. Rev. Lett.*, 2012, **108**, 215501.

[11] N. Xiong, S. Jiang, Y. Li, L. Tan and R. Li, *Appl. Phys. Lett.* 2008, **93**, 232905.

[12] T. Tubchareon, S. Soisuwan, S. Ratanathammaphan and P. Praserthdam, *J. Lumin.*, 2013, **142**, 75.

[13] M. G. Helander, Z. B. Wang, J. Qiu, M. T. Greiner, D. P. Puzzo, Z. W. Liu and Z. H. Lu, *Science*, 2011, **332**, 944.

[14] N. Zhou, D. B. Buchholz, G. Zhu, X. Yu, H. Lin, A. Facchetti, T. J. Marks and R. P. H. Chang, *Adv. Mater.*, 2014, **26**, 1098.

[15] M. Kato, T. Cardona, A. W. Rutherford and, E. Reisner, *J. Am. Chem. Soc.*, 2012, **134**, 8332.

[16] K. Ellmer, *Nat. Photonics*, 2012, **6**, 809.

[17] W. Mao, B. Xiong, Y. Liu and C. He, *Appl. Phys. Lett*., 2013, **103**, 031915.

[18] V. Consonni, G. Rey, H. Roussel, B. Doisneau, E. Blanquet and D. Bellet, *Acta Mater*., 2013, **61**, 22.

[19] J. Montero, J. Herrero and C. Guillén, *Sol. Energy Mater. Sol. Cells*, 2010, **94**, 612.

[20] S. Yu, W. Zhang, L. Li, D. Xu, H. Dong and Y. Jin. *Acta Mater.*, 2013, **61**, 5429.

[21] S. Yu, L. Ding, C. Xue, L. Chen and W. F. Zhang, *J. Non–Cryst. Solids*, 2012, **358**, 3137.

[22] H. Khassaf, N. Khakpash, F. Sun, N. M. Sbrockey, G. S. Tompa, T. S. Kalkur and S. P. Alpay, *Appl. Phys. Lett.*, 2014, **104**, 202902.

[23] W. J. Kim, W. Chang, S. B. Qadri, J. M. Pond, S. W. Kirchoefer, D. B. Chrisey and J. S. Horwitz, *Appl. Phys. Lett.*, 2000, **76**, 1185.

[24] A. Podpirka, M. W. Cole and S. Ramanathan, *Appl. Phys. Lett.*, 2008, **92**, 212906.

[25] W. G. Driscoll and W. Vaughan, Handbook of Optics, McGraw–Hill, USA (1978).

[26] K. Kuriyama, Y. Takahashi and F. Sunohara, *Phys. Rev. B*, 1993, **48**, 2781.

[27] J. S. Horwitz, W. Chang, W. Kim, S. B. Qadri, J. M. Pond, S. W. Kirchoefer and D. B. Chrisey, *J. Electroceram.*, 2000, **4**, 357.

[28] M. W. Cole, A. Podpirka and S. Ramanathan, *J. Mater. Sci.*, 2009, **44**, 5332.

[29] M. W. Cole, C. Hubbard, E. Ngo, M. Ervin, M. Wood and R. G. Geyer, *J. Appl. Phys.*, 2002, **92**, 475.

[30] K. M. Johnson, *J. Appl. Phys*., 1962, **33**, 2826.

[31] A. F. Devonshire, *Philos. Mag.*, 1949, **40**, 1040.

[32] S. Yu, L Li, N. Zhang, H. Dong, D. Xu and W. Zhang, *J. Alloys Compds.*, 2014, **612**, 26.

[33] J. S. Horwitz, W. Chang, W. Kim, S. B. Qadri, J. M. Pond, S. W. Kirchoefer and D. B. Chrisey, *J. Electroceram*., 2000, **4**, 357.

[34] J. Park, C. S. Hwang and D. Y. Yang, *J. Mater. Res*., 2001, **16**, 1363.

[35] Y. Guo, D. Akai, K. Sawada, M. Ishida and M. Gu, *J. Sol–Gel. Sci. Tech.*, 2009, **49**, 66.

[36] P. C. Joshy and S. B. Desu, *J. Appl. Phys*., 1996, **80**, 2349

Captions of figures

Figure 1. (a) Schematic drawings of the fully transparent thin–film varactors. (b) X–ray diffraction (θ–2θ) patterns of the as–deposited BST thin films and the annealed BST thin films.

Figure 2. (a) Transmittance spectra of the two sets of BST thin films; (b) Optical band gap of the e two sets of BST thin films; (c) Optical transmission spectrum of the two sets of ATO/Ag/BST/ATO/ quartz devices.

Figure 3. (a, b), DC bias field dependences of the capacitance and loss tangent of two sets of ATO/Ag/BST/ATO/quartz devices measured at a temperature of 20 °C and a frequency of 100 kHz. The experimental data of capacitance were fitted following Johnson's formula (solid lines); (c) The P–E loops of annealed BST thin films measured at room temperature; (d) The Leakage current density of the two sets of ATO/Ag/BST/ATO/quartz devices.

Figure 4. Capacitance and loss tangent as a function of frequency for the fully transparent thin–film varactors with annealed BST thin films.

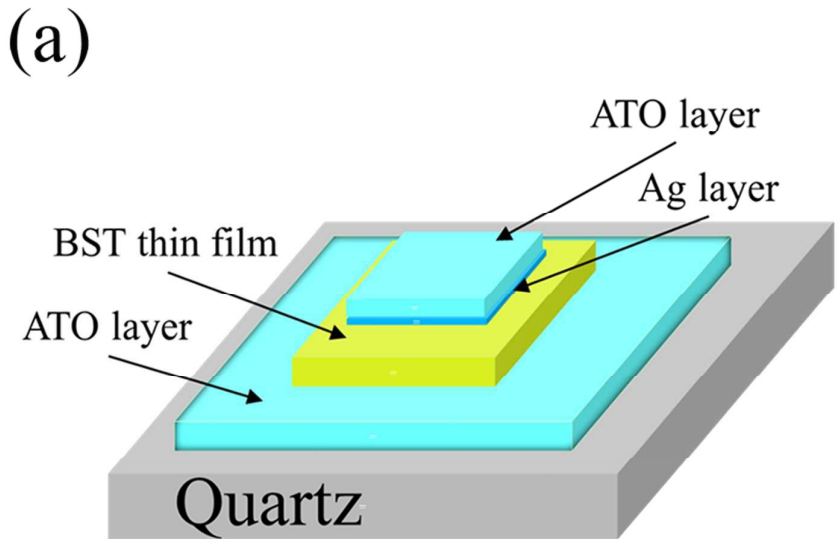

Figure 1(a)

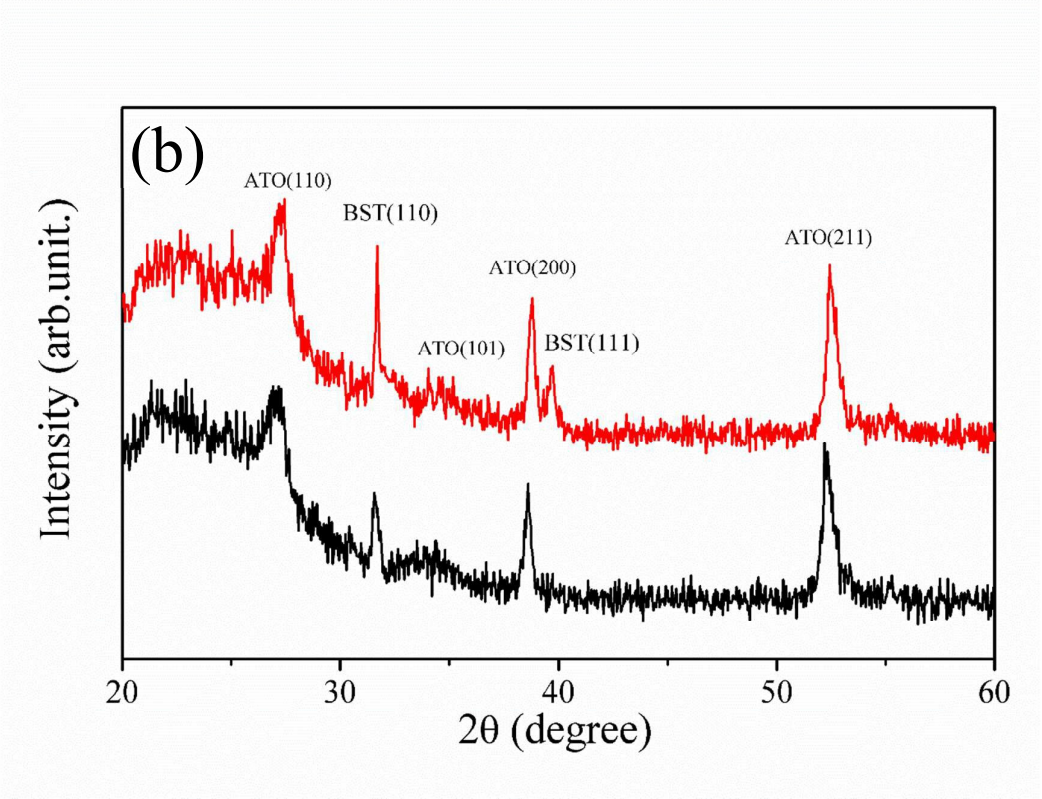

Figure 1(b)

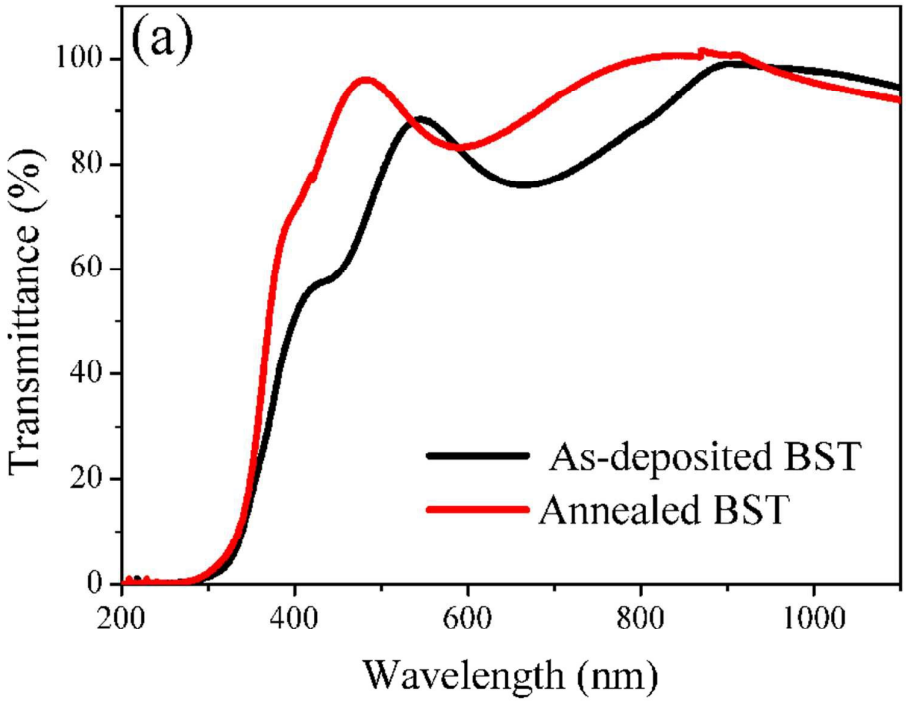

Figure 2(a)

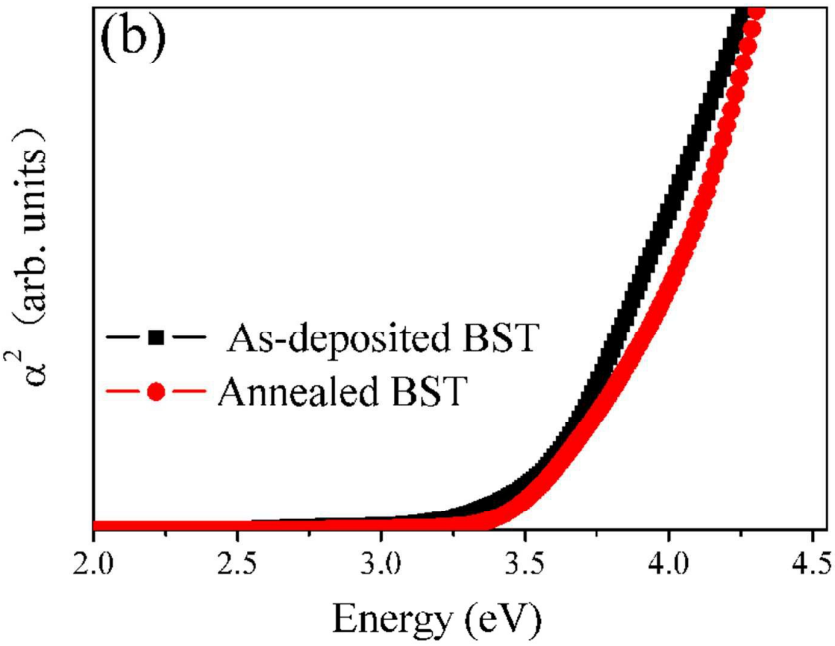

Figure 2(b)

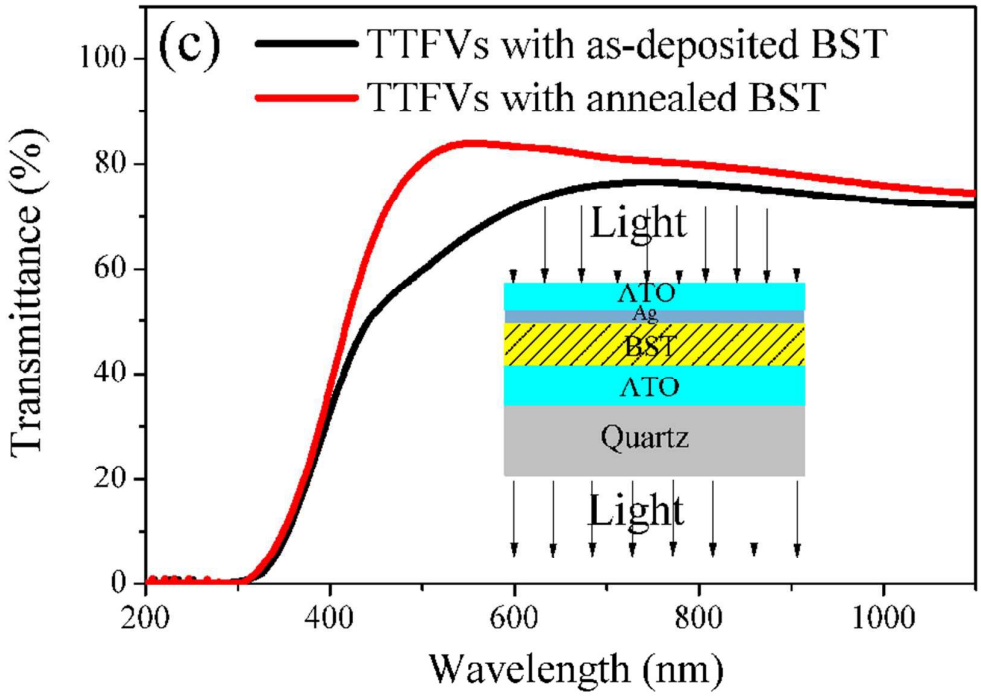

Figure 2(c)

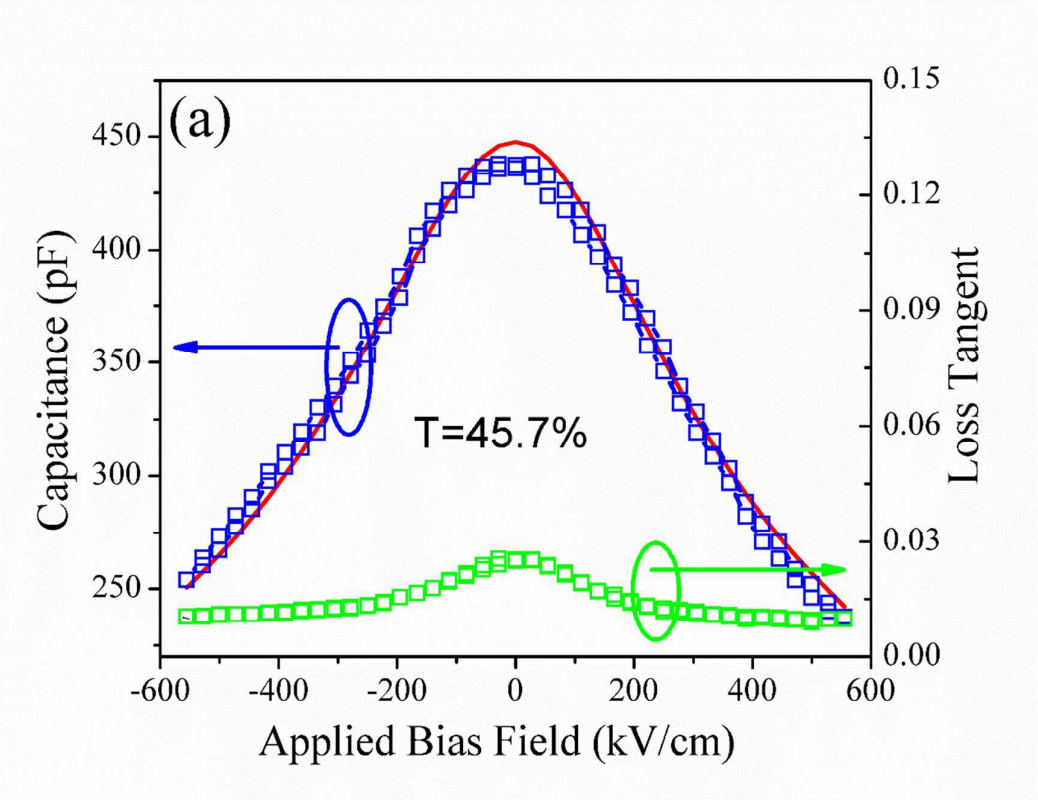

Figure 3(a)

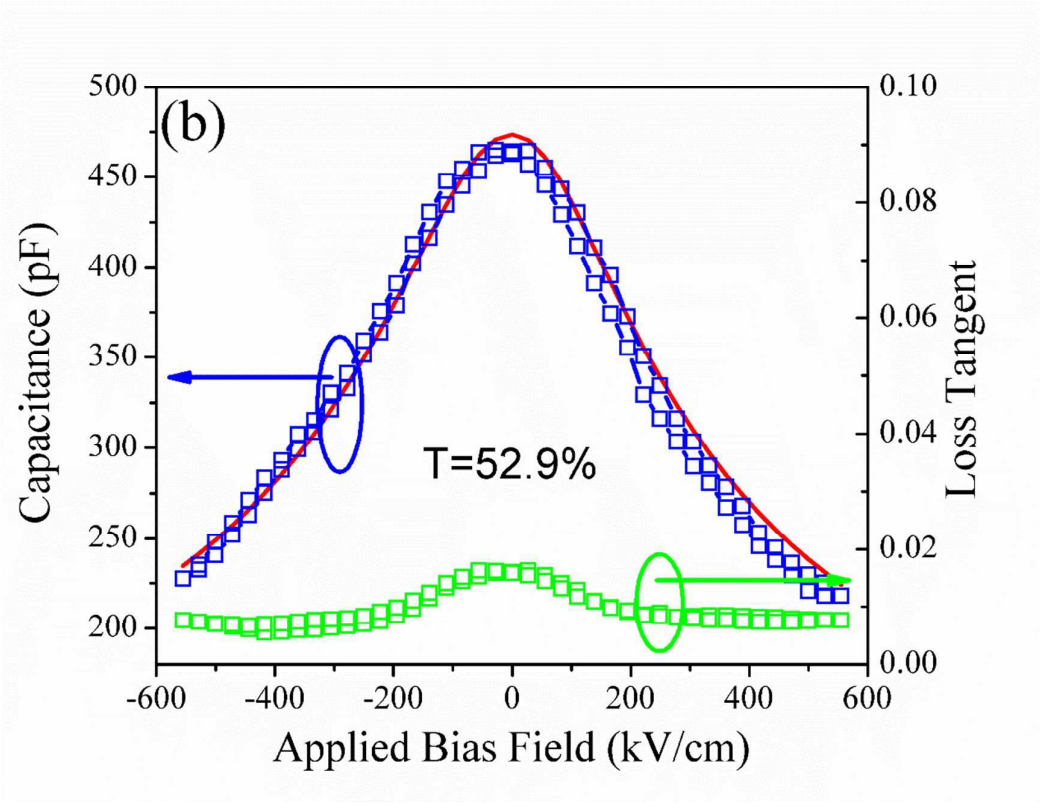

Figure 3(b)

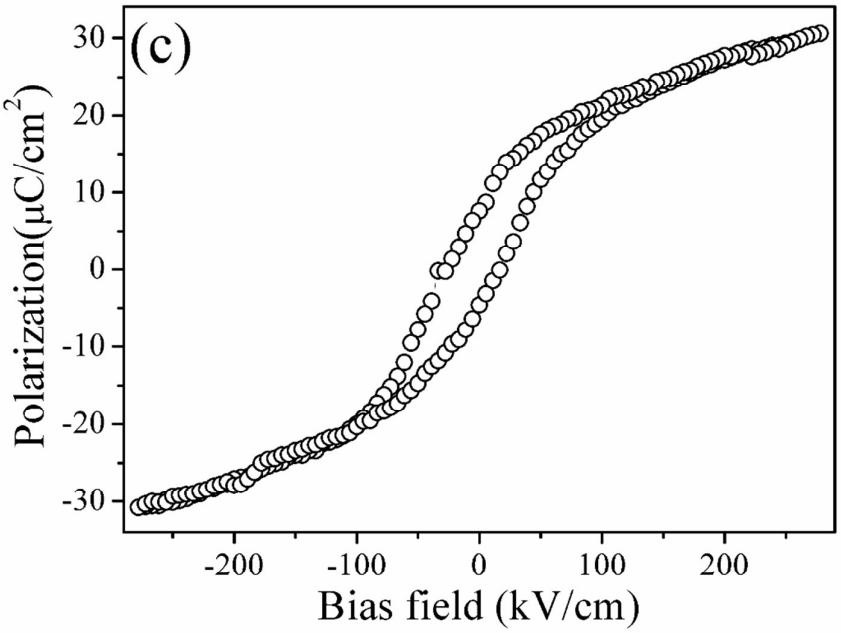

Figure 3(c)

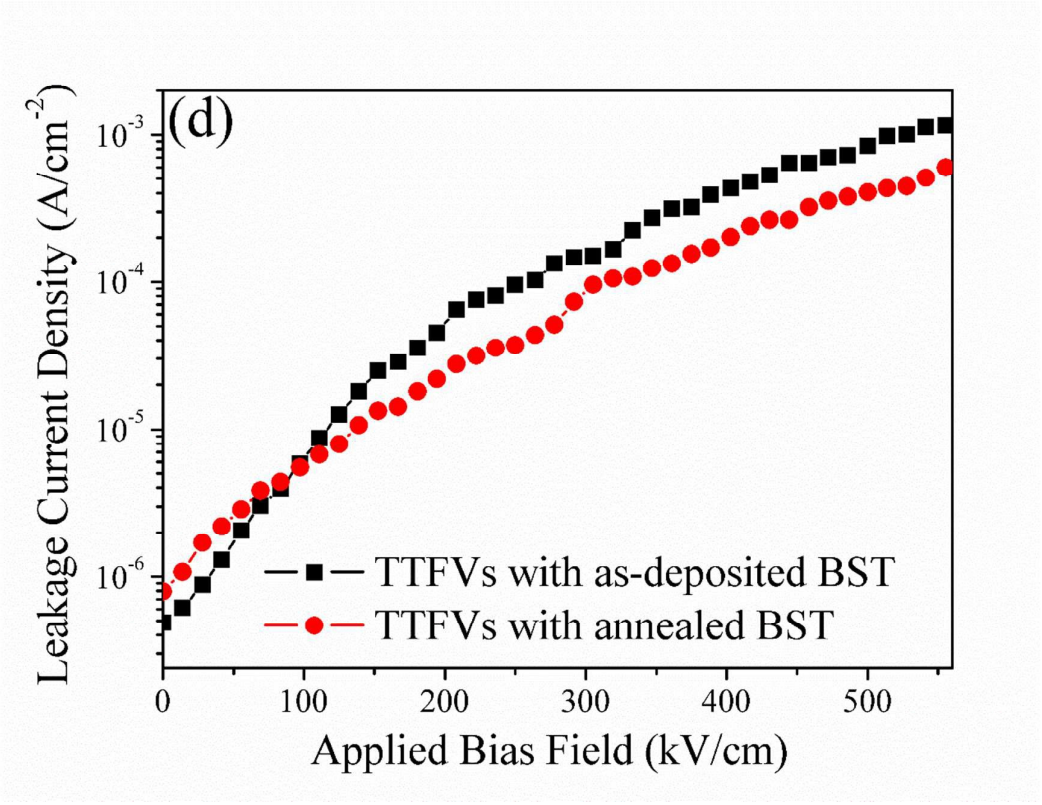

Figure 3(d)

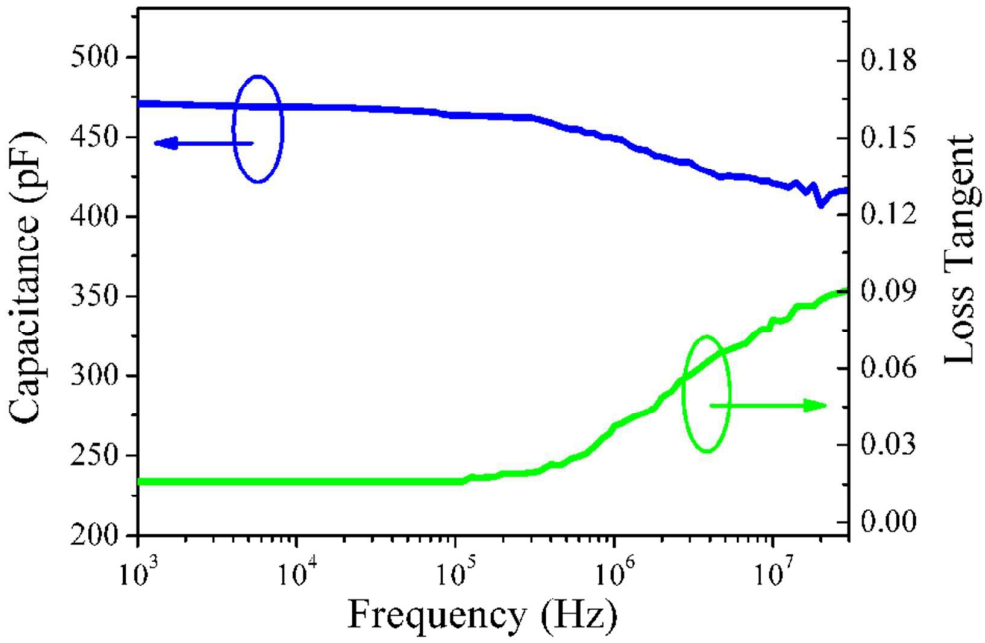

Figure 4

Table I. A comparison of the tunable characteristics of TTFVs, $Au/Ba_{0.6}Sr_{0.4}TiO_3/Au$ and $Au/Ba_{0.5}Sr_{0.5}TiO_3/Pt$ varactors.

	FOM	**Tunability**	**Loss tangent**	**E(kV/cm)**
ATO/Ag/BST/ATO $_{(annealed)}$	66	53%	0.008	560
ATO/Ag/BST/ATO $_{(as-deposited)}$	46	46%	0.010	560
$Au/Ba_{0.6}Sr_{0.4}TiO_3/Au$[a]	47	57%	0.012	670
$Au/Ba_{0.5}Sr_{0.5}TiO_3/Pt$[b]	35	54%	0.015	1200

[a]Reference 32 and [b]Reference 11